

Superradiance Lattice

Da-Wei Wang,^{1,2,*} Ren-Bao Liu,^{2,†} Shi-Yao Zhu,^{2,3} and Marlan O. Scully^{1,4,5}

¹Texas A&M University, College Station, TX 77843, USA

²Department of Physics and Centre for Quantum Coherence,
The Chinese University of Hong Kong, Hong Kong, China

³Beijing Computational Science Research Centre, Beijing 100084, China

⁴Princeton University, Princeton, New Jersey 08544, USA

⁵Baylor University, Waco, TX 76706, USA

(Dated: March 28, 2014)

We show that the timed Dicke states of a collection of three-level atoms can form a tight-binding lattice in the momentum space. This lattice, coined the superradiance lattice (SL), can be constructed based on an electromagnetically induced transparency (EIT) system. For a one-dimensional SL, we need the coupling field of the EIT system to be a standing wave. The detuning between the two components of the standing wave introduces an effective electric field. The quantum behaviours of electrons in lattices, such as Bloch oscillations, Wannier-Stark ladders, Bloch band collapsing and dynamic localization can be observed in the SL. The SL can be extended to two, three and even higher dimensions where no analogous real space lattices exist and new physics are waiting to be explored.

PACS numbers: 42.50.Nn, 61.50.Ah

Introduction.—From the early days of quantum mechanics, periodic lattice has been a platform for versatile quantum phenomena of electrons, such as Bloch oscillations [1, 2], Wannier-Stark ladders [3], and dynamic localization [4, 5] among many others. Although the fast dissipations prevent these phenomena from being observed in crystalline solids (except in superlattices [6, 7]), the development in optical lattice enables the observation of Bloch oscillations [8] and Wannier-Stark ladder [9] for cold atoms. The evidence of dynamic localization and Bloch band collapsing [10] under periodic forces were also observed in optical lattices [11] and photonic structures [12]. This Floquet dynamics becomes a hot topic recently because of its various applications in quantum phase transitions [13–16], Majorana fermions [17, 18], topological insulators [19–21], artificial gauge potentials [22–24] and edge states [25, 26]. Nevertheless, these phenomena are mostly based on optical lattices and their observations remain challenging. Novel types of lattices are therefore desirable to provide new testing grounds for the rich physics mentioned above.

In this Letter, we introduce the concept of superradiance lattice (SL), a lattice in the momentum space. The conventional lattice has discrete translational symmetry in the position space. The tight-binding model which allows electron hopping between nearest neighbours is diagonal in the momentum space. The crystal momentum \mathbf{k} is a good quantum number to label each eigenstate. Recently, new types of crystals in time domain [27–29] and in phase space [30] attracted a lot of interest. The SL corresponds to a tight-binding model in the momentum space which has good quantum numbers \mathbf{r} in the position space. The dynamics of \mathbf{r} in the SL is analogous to the dynamics of \mathbf{k} in the real space lattice. We show that the Bloch oscillations, Wannier Stark ladders

and Bloch band collapsing can be observed based on an electromagnetically induced transparency (EIT) system.

The momentum transfer between a single two-level atom and a standing wave light is quantized. The states of the atom with quantized recoil momenta thus have discrete translational symmetry in the momentum space. To inhibit the recoil motions, we can use fixed three-level systems in solids, which effectively have infinite mass thanks to the Mössbauer effect [31]. The phase correlations of the timed Dicke states, rather than the recoil momentum of single atoms, set the lattice points in the momentum space.

0D Dicke spinor.—A collection of N two-level atoms coupled by a single electromagnetic (EM) mode is described by the Dicke model [32]. If the atoms are randomly distributed in an area much larger than the wavelength, the first excited state which is the so-called timed Dicke state [33] can record the momentum of the photon via phase correlations between excited atoms,

$$|e_{\mathbf{k}_p}\rangle = \frac{1}{\sqrt{N}} \sum_{q=1}^N e^{i\mathbf{k}_p \cdot \mathbf{r}_q} |E_q\rangle. \quad (1)$$

Here \mathbf{k}_p is the wave vector of the photon, \mathbf{r}_q is the position of the q th atom, and $|E_q\rangle \equiv |g_1, g_2, \dots, e_q, \dots, g_N\rangle$, where g_q (or e_q) means that the q th atom is in the state $|g\rangle$ (or $|e\rangle$). The atomic levels are shown in the inset of Fig. 1 (a). Now we apply another EM plane wave mode \mathbf{k}_1 that couples $|e\rangle$ to a metastable state $|m\rangle$ via the interaction Hamiltonian (under the rotating wave approximation) $H_I = \sum_{q=1}^N \hbar t_1 a_1 e^{i\mathbf{k}_1 \cdot \mathbf{r}_q} |e_q\rangle \langle m_q| + h.c.$, where a_1 is the annihilation operator of mode \mathbf{k}_1 , t_1 is the vacuum coupling strength and is assumed to be real for simplicity. Then $|e_{\mathbf{k}_p}, n_1\rangle$ is coupled to $|m_{\mathbf{k}_p - \mathbf{k}_1}, n_1 + 1\rangle$ where n_1 is the photon number of mode \mathbf{k}_1 , and $|m_{\mathbf{k}_p - \mathbf{k}_1}\rangle$ is defined

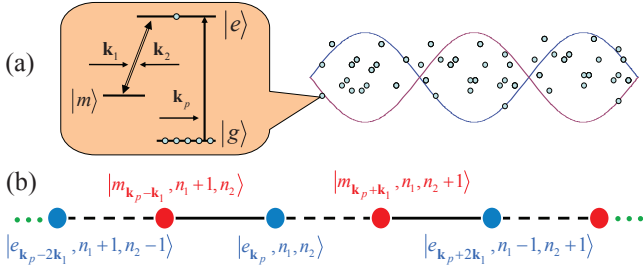


FIG. 1: (Color online) (a) The real space configuration and the internal atomic states of a 1D bipartite SL. An EM plane wave mode \mathbf{k}_p collectively excites the transition from $|g\rangle$ to $|e\rangle$. The standing wave formed by modes \mathbf{k}_1 and \mathbf{k}_2 couples the transition between $|e\rangle$ and $|m\rangle$. (b) The 1D bipartite SL in the momentum space. The red (blue) circles represent the $|m_{\mathbf{k}}\rangle$ ($|e_{\mathbf{k}}\rangle$) states. The solid (dash) lines represent the interaction via mode \mathbf{k}_1 (\mathbf{k}_2). The distance between the adjacent sites is $|\mathbf{k}_1|$ and the direction of \mathbf{k}_1 is defined to the right.

by replacing e (E) with m (M) in Eq. (1). The coupling strength $\hbar t_1 \sqrt{n_1 + 1}$ is the Rabi splitting between $|e_{\mathbf{k}_p}, n_1\rangle$ and $|m_{\mathbf{k}_p - \mathbf{k}_1}, n_1 + 1\rangle$. This splitting is independent of the atom number N . The two-states $|e_{\mathbf{k}_p}, n_1\rangle$ and $|m_{\mathbf{k}_p - \mathbf{k}_1}, n_1 + 1\rangle$ forms a zero-dimensional (0D) two-component Dicke spinor.

1D bipartite SL.—By introducing a second mode $\mathbf{k}_2 = -\mathbf{k}_1$, the interaction Hamiltonian

$$H_I = \sum_{q=1}^N \hbar(t_1 a_1 e^{i\mathbf{k}_1 \cdot \mathbf{r}_q} + t_2 a_2 e^{i\mathbf{k}_2 \cdot \mathbf{r}_q}) |e_q\rangle \langle m_q| + h.c., \quad (2)$$

extends the 0D Dicke spinor to a 1D bipartite SL, as shown in Fig. 1 (a). The state $|e_{\mathbf{k}_p}, n_1, n_2\rangle$ can be coupled either by mode \mathbf{k}_1 to $|m_{\mathbf{k}_p - \mathbf{k}_1}, n_1 + 1, n_2\rangle$ with coupling strength $\hbar t_1 \sqrt{n_1 + 1}$, or by mode \mathbf{k}_2 to $|m_{\mathbf{k}_p + \mathbf{k}_1}, n_1, n_2 + 1\rangle$ with coupling strength $\hbar t_2 \sqrt{n_2 + 1}$, as shown in Fig. 1 (b). The coupling strengths are site-dependent. However, if the two fields are in coherent states with large average photon numbers $\langle n_i \rangle \gg 1$ ($i = 1, 2$), the coupling strengths are approximately constant $\hbar \Omega_i = \hbar t_i \sqrt{\langle n_i \rangle}$. We can rewrite the single excitation interaction Hamiltonian of Eq. (2) in the tight-binding form,

$$H_I = \sum_j \hbar \Omega_1 \hat{e}_{2j}^\dagger \hat{m}_{2j-1} + \hbar \Omega_2 \hat{m}_{2j+1}^\dagger \hat{e}_{2j} + h.c., \quad (3)$$

where we have defined the creation operators

$$\hat{e}_j^\dagger (\hat{m}_j^\dagger) = \frac{1}{\sqrt{N}} \sum_{q=1}^N e^{i(\mathbf{k}_p + j\mathbf{k}_1) \cdot \mathbf{r}_q} |E_q(M_q)\rangle \langle G|, \quad (4)$$

with $|G\rangle \equiv |g_1, g_2, \dots, g_N\rangle$ the ground state and the superradiant states $|e_{\mathbf{k}_p + j\mathbf{k}_1}\rangle = \hat{e}_j^\dagger |G\rangle$.

The tight-binding model in momentum space is diagonal in its reciprocal position space. For simplicity, we let

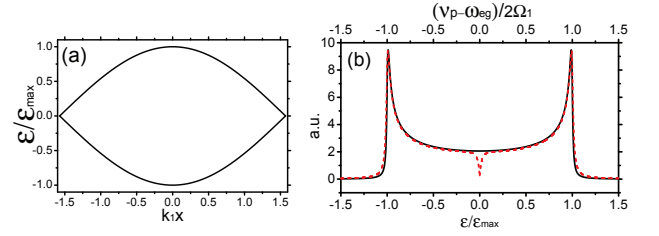


FIG. 2: (Color online) (a) The dispersion relation of a 1D SL. (b) The DOS of the SL (black solid) and the standing wave coupled EIT absorption spectrum (red dash). Here $\epsilon_{\max} = 2\Omega_1$ and the EIT decoherence rate is $\gamma = 0.06\Omega_1$. Assuming that each eigenstate has a finite life time, the DOS is Lorentzian broadened with width $0.01\epsilon_{\max}$ to fit with the EIT absorption spectrum. The two lines overlap except at the zero energy point, where the absorption is zero due to EIT effect.

$\Omega_1 = \Omega_2$. The dispersion relation is

$$\epsilon_{\pm}(\mathbf{r}) = \pm 2\hbar\Omega_1 \cos(\mathbf{r} \cdot \mathbf{k}_1), \quad (5)$$

as shown in Fig. 2 (a). The energy band is directly shown by the interference pattern of the coupling standing wave.

Detection by the standing wave coupled EIT.—Levels $|e\rangle$ and $|m\rangle$ are resonantly coupled by EM modes \mathbf{k}_1 and \mathbf{k}_2 . A weak field \mathbf{k}_p (in the single photon limit) which probes the transition from the ground state $|g\rangle$ to level $|e\rangle$ should create excitations in the 1D SL. The density of states (DOS) of the SL, $D(\epsilon) = N/\pi\sqrt{\epsilon_{\max}^2 - \epsilon^2}$ with $\epsilon_{\max} = 2\hbar\Omega_1$, can therefore be tested by the absorption spectrum of \mathbf{k}_p , which on the other hand can be got from the imaginary part of the EIT susceptibility,

$$\chi(x) = \frac{6\pi\mathcal{N}\Delta_p\gamma}{\Delta_p(\Delta_p - i\gamma) - |\Omega_1 e^{ik_1 x} + \Omega_2 e^{-ik_1 x}|^2}. \quad (6)$$

Here \mathcal{N} is the atomic numbers in the volume k_p^{-3} , γ is the decoherence rate between $|e\rangle$ and $|g\rangle$, $\Delta_p = \omega_{eg} - \nu_p$ is the detuning of the probe field, and we have assumed the decoherence rate between $|g\rangle$ and $|m\rangle$ is zero.

The absorption in Eq. (6) is periodic in space. The total absorption spectrum can be got by averaging Eq. (6) over one period,

$$A(\nu_p) \propto \text{Im} \left[\frac{k_1}{\pi} \int_{-\frac{\pi}{2k_1}}^{\frac{\pi}{2k_1}} \chi(x) dx \right]. \quad (7)$$

In Fig. 2, we plotted the density of states D and the absorption spectrum A . Their overlap demonstrates the equivalence between the 1D SL and the standing wave coupled EIT. The major difference is that the absorption spectrum A has a transparency point at zero detuning due to the EIT effect.

Effective electric field in the momentum space.—An effective electric field should introduce a potential linear with the momenta of the sites in an SL. From Fig.

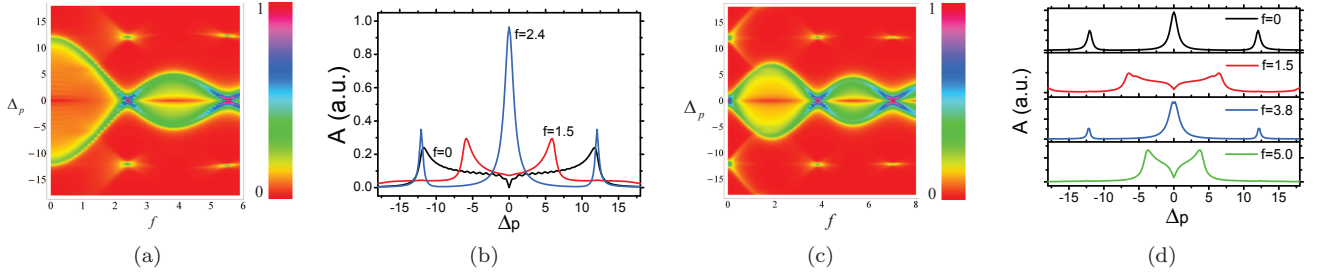


FIG. 3: (Color online) The absorption spectrum of a Λ -type EIT system driven by two counter-propagating modes with time-dependent frequencies, which is equivalent to a bipartite SL in a dynamic electric field. (a) Absorption spectra as function of detuning Δ_p and the amplitude-frequency ratio of the effective ac electric field f . $\delta_1 = \delta_2 = 0$ (which corresponds to a zero static electric field). The band collapses at the Bessel function zeros $J_0(f) = 0$ for $f = 2.4$ and 5.5 . (b) Absorption spectra for $f = 0$ (black), $f = 1.5$ (red), and $f = 2.4$ (blue) in (a). (c) Absorption spectra for $\delta_1 = -\delta_2 = \nu_d$ as a function of Δ_p and f . The band collapses at the Bessel function zeros $J_1(f) = 0$ for $f = 3.8$ and 7.0 . (d) Absorption spectra for $f = 0$ (black), $f = 1.5$ (red), $f = 3.8$ (blue), and $f = 5.0$ (green) in (c). The other parameters are $\Omega_1 = \Omega_2 = 6\gamma$, $\nu_d = 12\gamma$, $\gamma = 1$, and $\gamma' = 0.001$.

1 (b), we see that the superradiant states are attached with photon numbers that are linear with the momenta. We therefore can introduce an effective electric field by changing the energy of the photons of the two modes. The unperturbed Hamiltonian is

$$H_0 = \sum_{j=1}^N \hbar\omega_e |e_j\rangle \langle e_j| + \hbar\omega_m |m_j\rangle \langle m_j| + \hbar\nu_1 a_1^\dagger a_1 + \hbar\nu_2 a_2^\dagger a_2, \quad (8)$$

where $\hbar\omega_i$ ($i = e, m$) is the atomic eigenenergy and ν_i ($i = 1, 2$) is the angular frequency of the fields. The energy difference between $|e_{\mathbf{k}_p}, n_1, n_2\rangle$ and $|m_{\mathbf{k}_p - \mathbf{k}_1}, n_1 + 1, n_2\rangle$ is $\hbar\delta_1 = \hbar\omega_{em} - \hbar\nu_1$ where $\omega_{em} = \omega_e - \omega_m$, and the energy difference between $|e_{\mathbf{k}_p}, n_1, n_2\rangle$ and $|m_{\mathbf{k}_p + \mathbf{k}_1}, n_1, n_2 + 1\rangle$ is $\hbar\delta_2 = \hbar\omega_{em} - \hbar\nu_2$. The quantity $\hbar\delta_0 = \hbar\omega_{em} - \frac{1}{2}(\nu_1 + \nu_2)$ is the energy difference between the two sublattices of $|e\rangle$ and $|m\rangle$. The detuning between two fields $2\delta = \nu_1 - \nu_2$ gives the energy gradient of an effective electric field in the SL,

$$\mathbf{E} = \frac{\hbar\delta}{qk_1} \hat{\mathbf{k}}_1, \quad (9)$$

where q is the effective charge. $\hat{\mathbf{k}}_1$ is the unit vector along \mathbf{k}_1 . Therefore, the effective Hamiltonian is

$$H = \sum_j \hbar(\delta_0 - 2j\delta) \hat{e}_{2j}^\dagger \hat{e}_{2j} - \hbar(2j+1) \delta \hat{m}_{2j+1}^\dagger \hat{m}_{2j+1} + \left(\hbar\Omega_1 \hat{e}_{2j}^\dagger \hat{m}_{2j-1} + \hbar\Omega_2 \hat{m}_{2j+1}^\dagger \hat{e}_{2j} + h.c. \right). \quad (10)$$

The equation of motion of the position operator \mathbf{r} is

$$\dot{\mathbf{r}} = \frac{1}{i\hbar} [\mathbf{r}, -q\mathbf{E} \cdot \mathbf{k}] = \frac{-q\mathbf{E}}{\hbar} = -\frac{\delta}{k_1} \hat{\mathbf{k}}_1. \quad (11)$$

It is easy to understand this equation in real space. The detuning of the two counter-propagating plane wave fields leads to a moving standing wave with velocity $\frac{\delta}{k_1} \hat{\mathbf{k}}_1$.

By adiabatic following, the point \mathbf{r} will move with the velocity in Eq. (11). After time $T = \pi/\delta$, the standing wave moves a period $\lambda_1/2 = \pi/k_1$ and the system recovers its original state, which is the Bloch oscillation in the SL.

Bloch band collapsing.—If the effective electric field is periodic in time, the band collapsing may occur [5, 10, 34]. We make the frequencies of the two fields time-dependent, $\nu_i + \Delta_i \cos \nu_d t$ ($i = 1, 2$), which introduces an oscillating effective electric field in the SL. In particular for $\delta_1 = -\delta_2 = n\nu_d$ with integer n and $\Delta_2 = -\Delta_1$, the excitation in the SL is driven by an effective electric field $E = E_s + E_d \cos \nu_d t$ with static component $E_s = -\hbar\nu_d/qk_1$ and dynamic component $E_d = \hbar\Delta_1/qk_1$. The quasienergy band is [34]

$$\epsilon_n(x) = \pm 2\Omega_1 J_n(f) \cos(xk_1), \quad (12)$$

where $J_n(f)$ is the n th order Bessel function of the first kind and $f = \Delta_1/\nu_d$. One interesting feature of this Floquet quasienergy band is that it collapses at the zeros of $J_n(f)$.

Figure 3 (a) and (b) show the EIT absorption spectrum associated with the quasienergy bands for $n = 0$ (detailed calculations are in the Supplementary Material). At $f = 0$, the absorption spectrum has a broad DOS of a bipartite lattice. Increasing f leads to a narrower energy band following $J_0(f)$ and finally the energy band collapses at $f = 2.4$, where a strong absorption peak appears at the zero detuning. The separation between the Floquet energy bands $\nu_d = 2\Omega_1$ is large and the interaction between the states from different bands is weak. Therefore, most of the upper and lower Floquet bands are not visible. However, near the band collapsing points $f = 2.4$, the two Floquet sidebands is vaguely visible due to the large DOS. This band collapse effect has important consequence in control of atoms in real and momentum spaces. In the real space, the atoms at different positions recover their original transition frequency, although the standing wave breaks the continuous translational sym-

metry. In the momentum space, the timed Dicke states have zero group velocity in a flat band, which leads to the dynamic localization in momentum space.

The Wannier-Stark ladder appears if the field has a static part. In Fig. 3 (c) and (d), we plot the absorption spectra for $n = 1$. If $f = 0$, the field is purely static, and there are only three peaks at $\Delta_p = 0, \pm 2\nu_d$. Although the Wannier-Stark ladder spacing is ν_d , only the points on the sublattice of $|e\rangle$ can be excited, and then the spacing becomes $2\nu_d$. The localized $|m_k\rangle$ states are dark states because there is no direct coupling between $|g\rangle$ and $|m\rangle$ and the indirect coupling is suppressed by the large energy difference between different sites. As f increases, we observe energy bands following Eq. (12) with $n = 1$. The bands collapse at the zero points of $J_1(f)$, $f = 3.8$ and 7.0 . These results are consistent with the results of electrons [35, 36]. The band collapsing for some other cases are discussed in the Supplementary Material.

Discussion.—The 1D SL is closely related to the electromagnetically induced grating (EIG) [37] where the n th order diffraction is emitted by the superradiant excitation $|e_{\mathbf{k}_p + n\mathbf{k}_1}\rangle$, which has been experimentally observed [38, 39]. Even the SL Wannier-Stark ladder has also been experimentally observed [40]. Although the experiment was explained by bichromatic EIT, it is equivalent to an SL in a static effective electric field. The dynamic localization can also be observed via similar experimental set up by periodically modulating the coupling field frequencies.

The SL can also be realized in cold atoms if the Doppler shift due to the recoil is much smaller than the coupling field Rabi frequency (see Supplementary Material). For example, we can choose ^{85}Rb D1 line with $|g\rangle = |5^2S_{1/2}, F = 2\rangle$, $|e\rangle = |5^2P_{1/2}, F = 2\rangle$ and $|m\rangle = |5^2S_{1/2}, F = 3\rangle$. The decay rate $\gamma = 2\pi \times 5.75\text{MHz}$. For the parameters in Fig.3, the Rabi frequency $\Omega_1 = 6\gamma = 2\pi \times 34.5\text{MHz}$ (intensity 0.43W/cm^2) is much larger than the Doppler shift $2\pi \times 7.4\text{kHz}$. The modulation frequency $\nu_d = 12\gamma = 2\pi \times 69\text{MHz}$ and the modulation amplitude $\Delta_{1,2}$ should be in the range $0 \sim 400\text{MHz}$. The thermal motions of the atoms induce random electric fields. In the μK regime, this random motion brings energy shift $\sim\text{kHz}$, which is much smaller than the effective electric potential energy $\sim\text{MHz}$. The band collapsing can be directly observed through the absorption spectra.

The applications of SL's are promising. The transport of the superradiant excitations in SL's can be used to reflect high-frequency light (for example, x-ray or ultraviolet) with low-frequency light (visible light or infrared) [41]. The coupling strength between the lattice point is tunable, which allows us to prepare a superposition of two timed Dicke states that are far apart in the momentum space for Heisenberg limit metrology [42].

The 1D superradiance chain can be extended to a 2D honeycomb lattice by introducing three-mode coupling field with wave vectors $\mathbf{k}_1 = k(-\frac{1}{2}\hat{x} - \frac{\sqrt{3}}{2}\hat{y})$, $\mathbf{k}_2 = k\hat{x}$ and

$\mathbf{k}_3 = k(-\frac{1}{2}\hat{x} + \frac{\sqrt{3}}{2}\hat{y})$. Similarly, four-mode coupling field can construct diamond-structure tight-binding model. A particular interesting subject to be investigated in the future is the tight-binding SL in dimensions higher than three when the number of the coupling fields is more than four. Since real-space tight-binding models have at most three-dimensions, a wealth of new physics may emerge from the extra dimensions of SL. Another convenient advantage of the SL is that the energy band is directly determined by the interference pattern of the multi-mode coupling fields. The energy bands and the Berry phases can be directly imaged in the real space. This provides connection between the Berry phases and the optical currents [43]. A lot of interesting phenomena, such as the overlapping of EIT point and Dirac point in graphene, Berry phases, artificial gauge field, monopoles and momentum space quasicrystals will be discussed elsewhere.

In conclusion, we proposed the concept of superradiance lattices based on a standing wave coupled EIT system. An effective electric field can be introduced by the detuning between the two components of the standing wave. The Wannier-Stark ladder and the Bloch band collapsing can be observed from the absorption spectra of the probe field. The dynamic localization can be observed from the disappearance of the various diffraction orders in an EIG scheme. By introducing more EM modes, this lattice can be extended to higher dimensions where many interesting physics can be studied.

We gratefully acknowledge the support of the National Science Foundation Grant PHY-1241032 and the Robert A. Welch Foundation (Awards A-1261). R.B.Liu was supported by Hong Kong RGC Project 401011 and CUHK Focused Investments Scheme. S.-Y. Zhu was supported by NSFC1174026.

* Electronic address: cuhkwdw@gmail.com

† Electronic address: rblu@phy.cuhk.edu.hk

- [1] Bloch, F. *Zeitschrift für Physik* **52**(7-8), 555–600 (1929).
- [2] Zener, C. *Proceedings of the Royal Society of London. Series A* **145**(855), 523–529 (1934).
- [3] Wannier, G. H. *Physical Review* **117**(2), 432–439 (1960).
- [4] Ignatov, A. A. and Romanov, Y. A. *Physica Status Solidi B-Basic Research* **73**(1), 327–333 (1976).
- [5] Dunlap, D. H. and Kenkre, V. M. *Physical Review B* **34**(6), 3625–3633 (1986).
- [6] Leo, K., Bolivar, P. H., Brüggemann, F., Schwedler, R., and Köhler, K. *Solid State Communications* **84**(10), 943–946 (1992).
- [7] Lyssenko, V. G., Valušis, G., Löser, F., Hasche, T., Leo, K., Dignam, M. M., and Köhler, K. *Physical Review Letters* **79**(2), 301–304 (1997).
- [8] Ben Dahan, M., Peik, E., Reichel, J., Castin, Y., and Salomon, C. *Physical Review Letters* **76**(24), 4508–4511 (1996).
- [9] Wilkinson, S. R., Bharucha, C. F., Madison, K. W., Niu, Q., and Raizen, M. G. *Physical Review Letters* **76**(24),

- 4512–4515 (1996).
- [10] Holthaus, M. *Physical Review Letters* **69**(2), 351–354 (1992).
 - [11] Madison, K. W., Fischer, M. C., Diener, R. B., Niu, Q., and Raizen, M. G. *Physical Review Letters* **81**(23), 5093–5096 (1998).
 - [12] Szameit, A., Garanovich, I. L., Heinrich, M., Sukhorukov, A. A., Dreisow, F., Pertsch, T., Nolte, S., Tinnermann, A., Longhi, S., and Kivshar, Y. S. *Physical Review Letters* **104**(22), 223903 (2010).
 - [13] Eckardt, A., Weiss, C., and Holthaus, M. *Physical Review Letters* **95**(26), 260404 (2005).
 - [14] Lignier, H., Sias, C., Ciampini, D., Singh, Y., Zenesini, A., Morsch, O., and Arimondo, E. *Physical Review Letters* **99**(22), 220403 (2007).
 - [15] Zenesini, A., Lignier, H., Ciampini, D., Morsch, O., and Arimondo, E. *Physical Review Letters* **102**(10), 100403 (2009).
 - [16] Struck, J., Öschl ager, C., Le Targat, R., Soltan-Panahi, P., Eckardt, A., Lewenstein, M., Windpassinger, P., and Sengstock, K. *Science* **333**(6045), 996–999 (2011).
 - [17] Jiang, L., Kitagawa, T., Alicea, J., Akhmerov, A. R., Pekker, D., Refael, G., Cirac, J. I., Demler, E., Lukin, M. D., and Zoller, P. *Physical Review Letters* **106**(22), 220402 (2011).
 - [18] Liu, D. E., Levchenko, A., and Baranger, H. U. *Physical Review Letters* **111**(4), 047002 (2013).
 - [19] Kitagawa, T., Berg, E., Rudner, M., and Demler, E. *Physical Review B* **82**(23), 235114 (2010).
 - [20] Lindner, N. H., Refael, G., and Galitski, V. *Nat Phys* **7**(6), 490–495 (2011).
 - [21] Hauke, P., Tieleman, O., Celi, A., Ischlger, C., Simonet, J., Struck, J., Weinberg, M., Windpassinger, P., Sengstock, K., Lewenstein, M., and Eckardt, A. *Physical Review Letters* **109**(14), 145301 (2012).
 - [22] Struck, J., Öschl ager, C., Weinberg, M., Hauke, P., Simonet, J., Eckardt, A., Lewenstein, M., Sengstock, K., and Windpassinger, P. *Physical Review Letters* **108**(22), 225304 (2012).
 - [23] Aidelsburger, M., Atala, M., Lohse, M., Barreiro, J. T., Paredes, B., and Bloch, I. *Physical Review Letters* **111**(18), 185301 (2013).
 - [24] Miyake, H., Siviloglou, G. A., Kennedy, C. J., Burton, W. C., and Ketterle, W. *Physical Review Letters* **111**(18), 185302 (2013).
 - [25] G omez-Le on, A. and Platero, G. *Physical Review Letters* **110**(20), 200403 (2013).
 - [26] Rudner, M. S., Lindner, N. H., Berg, E., and Levin, M. *Physical Review X* **3**(3), 031005 (2013).
 - [27] Shapere, A. and Wilczek, F. *Physical Review Letters* **109**(16), 160402 (2012).
 - [28] Wilczek, F. *Physical Review Letters* **109**(16), 160401 (2012).
 - [29] Li, T., Gong, Z.-X., Yin, Z.-Q., Quan, H. T., Yin, X., Zhang, P., Duan, L. M., and Zhang, X. *Physical Review Letters* **109**(16), 163001 (2012).
 - [30] Guo, L., Marthaler, M., and Sch on, G. *Physical Review Letters* **111**(20), 205303 (2013).
 - [31] M ossbauer, R. *Zeitschrift f ur Physik* **151**(2), 124–143 (1958).
 - [32] Dicke, R. H. *Physical Review* **93**(1), 99–110 (1954).
 - [33] Scully, M. O., Fry, E. S., Ooi, C. H. R., and Wdkiewicz, K. *Physical Review Letters* **96**(1), 010501 (2006).
 - [34] Zak, J. *Physical Review Letters* **71**(16), 2623–2625 (1993).
 - [35] Zhao, X.-G. *Physics Letters A* **155**(45), 299–302 (1991).
 - [36] Liu, R.-B. and Zhu, B.-F. *Physical Review B* **59**(8), 5759–5769 (1999).
 - [37] Ling, H. Y., Li, Y.-Q., and Xiao, M. *Physical Review A* **57**(2), 1338–1344 (1998).
 - [38] Mitsunaga, M. and Imoto, N. *Physical Review A* **59**(6), 4773–4776 (1999).
 - [39] Cardoso, G. C. and Tabosa, J. W. R. *Physical Review A* **65**(3), 033803 (2002).
 - [40] Wang, J., Zhu, Y., Jiang, K. J., and Zhan, M. S. *Physical Review A* **68**(6), 063810 (2003).
 - [41] Wang, D.-W., Zhu, S.-Y., Evers, J., and Scully, M. O. *ArXiv 1305.3636* (2013).
 - [42] Wang, D.-W. and Scully, M. O. *ArXiv 1403.3647* (2014).
 - [43] Berry, M. V. *Journal of Optics A: Pure and Applied Optics* **11**(9), 094001 (2009).